

# A TESTING PROCEDURE FOR THE EVALUATION OF DIRECTIONAL MESH BIAS

A.T. Slobbe\*, M.A.N. Hendriks<sup>\*,†</sup>, J.G. Rots\*

\*Faculty of Civil Engineering and Geosciences, Delft University of Technology  
P.O. Box 5048, 2600 GA Delft, The Netherlands  
e-mail: a.t.slobbe@tudelft.nl (A.T. Slobbe)

<sup>†</sup>Norwegian University of science and technology (NTNU)  
Rich. Birkelandsvei 1A, 7491 Trondheim, Norway

**Key words:** Directional mesh bias, Concrete, Fracture, Finite elements, Crack band model

**Abstract.** This paper presents a dedicated numerical test that enables to assess the directional mesh bias of constitutive models in a systematic way. The test makes use of periodic boundary conditions, by which strain localization can be analyzed for different mesh alignments with preservation of mesh uniformity and with exclusion of boundary disturbances.

After an exploratory study of the proposed test, the test is demonstrated by applying it to the classical and still widely used crack band model. An analysis series is performed on five meshes with different alignments. The meshes consist of squared quadrilateral elements with varying interpolation function and numerical integration scheme. From the results it can be concluded that the test identifies a significant mesh-induced directional bias.

## 1 INTRODUCTION

When modeling strain localizations (e.g. [1]) with finite element (FE) discretizations and standard continuum models, generally mesh dependency is observed. The spatial discretization or mesh layout influences the numerical solution, and mesh objective energy dissipation of the fracture process cannot be guaranteed. The mesh dependency can be subdivided in a preference to propagation of the strain localization band along continuous mesh lines (*directional mesh bias*) and in a sensitivity with respect to the size of the finite element (*mesh size sensitivity*). Although the latter issue has been properly solved by the introduction of the crack band model [2], the directional mesh bias is still a challenging topic. To overcome this issue of mesh dependency many different solutions have been proposed. In the context of smeared crack

models one could think of adding nonlocal or gradient terms to the constitutive modelling, resulting in higher order continuum models. Apart from the continuum based models one could also think of models that include discontinuities, like the extended finite element method (X-FEM) and the concept of embedded discontinuities.

In order to assess the influence of directional mesh bias on the results when using one of the above models, authors usually perform analyses on one or more fracture tests. Very popular are the single-edge-notched (SEN) and double-edge-notched (DEN) specimens, uni-axial tension tests, strips with a hole and a three-point bending test. Commonly one compares the numerical results obtained from a structured versus an unstructured finite element mesh, or from a regular versus a slanted finite element mesh,

after which conclusions are drawn whether the directional bias of the mesh is eliminated or not. Without objecting to the correctness of these conclusions the authors propose to study the sensitivity with respect to the orientation of the crack versus the mesh lines in a more elaborated and systematic way. Therefore a dedicated numerical test is presented in this paper. Assessment of the constitutive models on directional mesh bias with this test may lead to a better understanding of the influence of the involved parameters, and possibly to improvement of model's ability to deal with it.

The test introduces the concept of periodicity [3] in the field of strain localization analysis. The idea is that a finite piece is cut from an assumed infinite, initially homogeneous, discretized periodic medium. Within a two-dimensional  $\mathbb{R}^2$  space the discretized periodic medium is represented by an infinite (flat) plane, see an example in Fig. 1, while in a three-dimensional  $\mathbb{R}^3$  space an infinite volume is used. The isolated finite plane or volume is now considered as a separate FE discretization with periodic length scales  $L_i$ ,  $i = x, y, z$ , by which constraints will be added at the opposite boundaries. When these constraints or periodic boundary conditions are properly assigned, the behavior of a finite plane/volume within an infinite periodic medium under certain loading conditions can be simulated exactly with the FE model of just the isolated finite plane/volume. Actually, knowing the behavior of the finite plane/volume also the behavior of the infinite medium is known, under the assumption of periodicity. Note that due to the imposed periodicity in principle it is not important how the boundary edges are shaped, since they do not have a physical meaning anymore, as long as they are periodic. This means that the distance between the opposite boundary edges/faces should be everywhere the same for each pair of edges/faces. The absence of physical boundaries in this numerical test may be particularly appealing for the nonlocal models and the gradient-enhanced models.

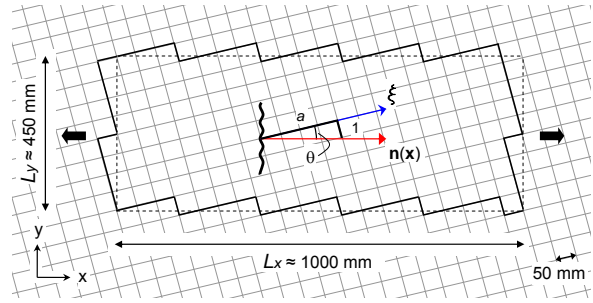


**Figure 1:** A possible geometry (2D) of a finite plane, taken from an infinite discretized periodic medium, with periodic length scales  $L_x$  and  $L_y$ , loaded by a uni-axial tensile load.

Including periodic boundary conditions, the numerical test enables to adopt different mesh alignments or element orientation angles  $\theta$  with respect to the loading direction. In contrast with standard tests this can be done without boundary disturbances on the localization process and with preservation of mesh uniformity. *Mesh uniformity* in this sense means that all characteristics of each finite element (i.e. shape, size, orientation, interpolation function and numerical integration scheme) in a specific mesh are identical. More details and some specific possibilities of the proposed test are described in another work of the authors [4].

In this paper the numerical test is used to assess the directional mesh bias of the classical and still widely used crack band approach [2] in the smeared cracking concept. Although the test can be used in three-dimensional models and with different loading cases as well, analyses are only performed for two-dimensional plane stress situations with uni-axial tensile loading. Section 2 presents the results of an exploratory study of the test with periodic boundary conditions. Subsequently, the results of a mesh alignment study are shown in Section 3.

## 2 EXPLORATORY STUDY

In this section the numerical test with periodic boundary conditions is explored by means of variations of the solution procedure, the softening law and the use of an imperfection. For all the performed analyses the same mesh is adopted. The geometry, boundary conditions

and material input of the test are given in Section 2.1. Section 2.2 presents results of the different analyses.

## 2.1 Modeling aspects

In Fig. 1 the general setup of the test is shown and the element orientation angle  $\theta$  is defined. For the analysis series described in this section a  $\theta$  - value of  $\pi/4$  is used. The geometry of the two-dimensional model is composed by periodic length scales  $L_x$  and  $L_y$  of 990 mm and 424 mm. The model is meshed with squared quadrilateral elements based on linear interpolation and with a  $2 \times 2$  Gauss integration order. A selective reduced integration is specified for the shear terms. Element sizes of 50 mm by 50 mm and a thickness  $t$  of 150 mm are adopted. Periodic boundary conditions are applied by the specification of linear dependencies between the degrees of freedom of the nodal pairs at the opposite edges, using a master-slave format. The numerical models are loaded by a uni-axial tensile load in the horizontal direction, represented by a constant displacement difference in x-direction between the left and right model boundaries.

The material behavior is modeled with an orthogonal fixed crack model and a variable shear retention relation [5]. A crack band model according to Govindjee et al. [6], based on Oliver [7] is used. The following fictitious material properties are adopted: a Young's modulus  $E_0$  of 10,000 N/mm<sup>2</sup>, a tensile strength  $f_t$  of 1.0 N/mm<sup>2</sup>, a material fracture energy  $G_f$  of 0.125 N/mm and a Poisson's ratio  $\nu$  of 0.0.

**Table 1:** List of performed analyses

	<i>sol. procedure</i>	<i>softening law</i>	<i>imperfection</i>
1.	SLA	Hordijk	no
2.	rNR	Hordijk	no
3.	SLA	Hordijk	yes
4.	rNR	Hordijk	yes
5.	SLA	Moelands	no
6.	SLA	Moelands	yes

In total six analyses are performed in this exploratory study, summarized in Table 1. Regarding the variations, in case of an applied imperfection the tensile strength  $f_t$  is reduced with 5% in one element. Furthermore, nonlinear stress - strain relations according to Hordijk [8] softening and Moelands & Reinhardt [9] softening are adopted, see Fig. 2. Based on the aforementioned material properties the crack openings  $w_{ult}$  at which stresses can no longer be transferred are 0.642 mm and 0.528 mm respectively. The Moelands & Reinhardt softening curve is characterized by its initial steep decreasing slope of  $-\infty$ . Finally, two different solution procedures are used: an incremental-iterative scheme based on a regular Newton - Raphson method (rNR), and the Sequentially Linear Analysis (SLA) method, e.g. [5, 10]. The last mentioned method replaces the standard incremental-iterative solution procedure by a series of scaled linear analyses. In every analysis a critical event is traced and subsequently a stiffness and strength reduction in the critical integration point is applied. In order to apply such damage increments a discretization of the nonlinear stress - strain relation is required, resulting in the use of a so-called saw-tooth curve with a finite number of damage increments. For the analyses in this paper the softening diagram is approximated by 20 damage increments.

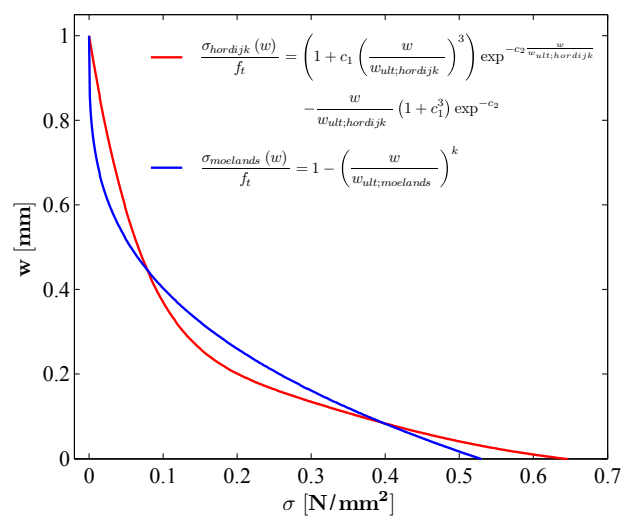


**Figure 2:** Hordijk and Moelands & Reinhardt softening laws for given material properties.

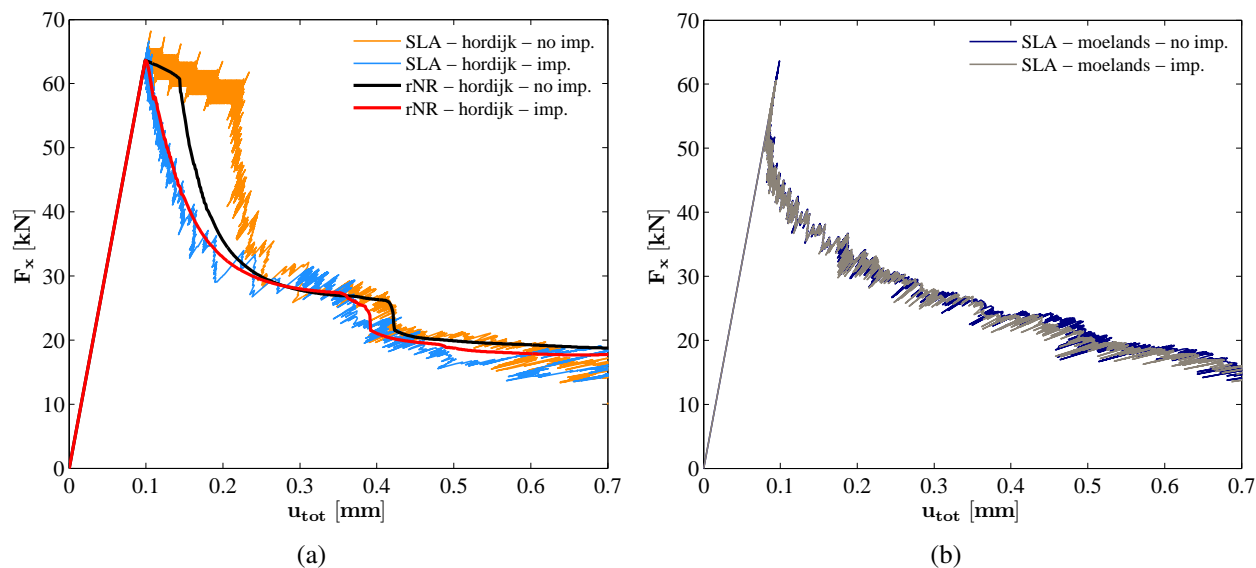


**Figure 3:** Load - displacement curves of analyses with Hordijk softening (a) and Moelands & Reinhardt softening (b).

## 2.2 Results

Fig. 3 presents the global responses of the six analyses in terms of load - displacement curves. Firstly, it can be seen that all numerically obtained curves show a ductile post-peak behavior with a residual plateau at about 15-20 kN. Subsequently, the curves of the corresponding rNR and SLA-analyses with Hordijk softening show reasonable agreement. The observed spiky shapes of the SLA curves are typical for the SLA method due to its saw-tooth softening input. Note that with respect to the rNR analyses almost all load increments are converged. Finally, the observed load drops in the curves coincide with ‘fast’ strain localizations, as will be shown below. For the analyses with Hordijk softening and without an imperfection this happens not immediate after the peak load has been reached. Their curves in Fig. 3(a) reveal first a plateau before the load drops and with that the strains localize in a small zone. For the comparable analysis with Moelands & Reinhardt softening in Fig. 3(b) strain localization occur right after the peak. This curve, on the other hand, shows even an snapback behavior. From the above mentioned observations it can be stated that all analyses suffer from stress locking [11]. In case of a fully developed single crack one could expect a  $F_x$  of zero when

$w_{ult}$  is reached. However, induced by misalignment of the crack band with the mesh lines spurious stresses across the crack occur, resulting in an asymptotic post-peak behavior to a certain load level. The height of this load level depends on the degree of misalignment. Furthermore, it is found that with Hordijk softening an immediate strain localization after the peak does not always occur. In case that no imperfection is added to the model, both rNR and SLA results show initial cracking of all the integration points in the model. This explains the plateau in the corresponding curves right after the peak, since all the integration points contribute to energy dissipation in the model. At a certain moment the strains localize in a relatively small part of the model, leading to unloading and crack closure in the remaining part. Fig. 4 shows this for the analysis ‘rNR - hordijk - no imp.’. The crack strain plot is taken at  $u_{tot} = w_{ult}$ . Note that the numerically obtained localization bandwidth is extended over approximately two columns of elements.

The addition of an imperfection in the model helps to trigger a ‘fast’ localization, as can be concluded from the immediate load drop right after the peak in Fig. 3(a). The crack plot just after the peak shows only one single macro crack in the model rather than micro-cracking

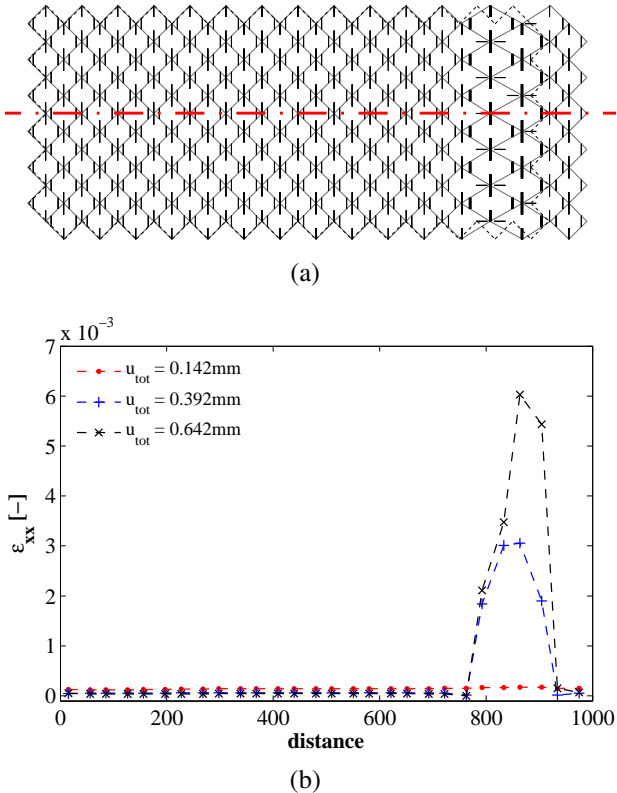


**Figure 4:** Crack strain plot (deformed mesh) at  $u_{tot} = 0.642\text{mm}$  (a) and evolution of strain profile (b) at red line in Fig. 4(a), belonging to analysis ‘rNR - hordijk - no imp.’.

in all integration points. This holds also true when a Moelands & Reinhardt softening is adopted, see Fig. 3(b). Strain localization is now stimulated by the initial steeper slope of the softening branch of the local constitutive relation, see Fig. 2. The addition of an imperfection appears superfluous in case of Moelands & Reinhardt softening, and this might be advantageous considering the concept of periodicity. Fig. 5 shows the strain profiles at  $u_{tot} = w_{ult}$  of both analyses with Moelands & Reinhardt softening. Two different locations of the strain localizations can be observed. In case of ‘SLA - moelands - imp.’ the location of the strain jump is in the middle (coinciding with the location of the applied imperfection), where in case of ‘SLA - moelands - no imp.’ the strains arbitrarily localize near the left and right model boundaries. In the initial homogeneous strain field this is determined by numerical round-off [12]. Note that, although not proven here, an imper-

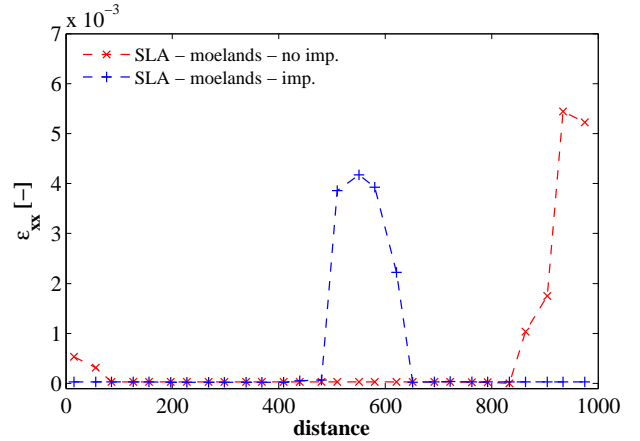


**Figure 5:** Strain profiles at  $u_{tot} = 0.528\text{mm}$  of SL-analyses with Moelands & Reinhardt softening in Fig. 3(b).

fection is inevitable in order to obtain ‘fast’ strain localizations with standard incremental-iterative solution procedures. For SLA this is not necessary, due to the adopted ‘‘event-by-event’’ strategy.

### 3 MESH ALIGNMENT STUDY

The mesh alignment study is performed with Moelands & Reinhardt softening, without imperfections *and* SLA as solution procedure. Variations are done with element types and mesh alignments or element orientations. Three different quadrilateral element types are used. The first one is a quadrilateral based on linear interpolation, with a  $2 \times 2$  Gauss integration order and a selective reduced integration for the shear terms. The second and third element types are quadrilateral eight-node elements based on quadratic interpolation and with a  $2 \times 2$  and  $3 \times 3$  Gauss integration order respectively. Furthermore, five different element orientation angles  $\theta$  are adopted, which are depicted in Fig. 6. The alignments are the result of five selected  $a$ -values, namely  $\infty$ , 9, 4, 2 and 1. From Fig. 1 it can be seen that the  $a$ -values arise from the geometry of the step-shaped boundary edges, and that they are directly coupled to  $\theta$ . All five FE discretizations are meshed with each of the three element types, resulting in 15 different *uniform* meshes. The remaining modeling aspects are the same as in Section 2.1.

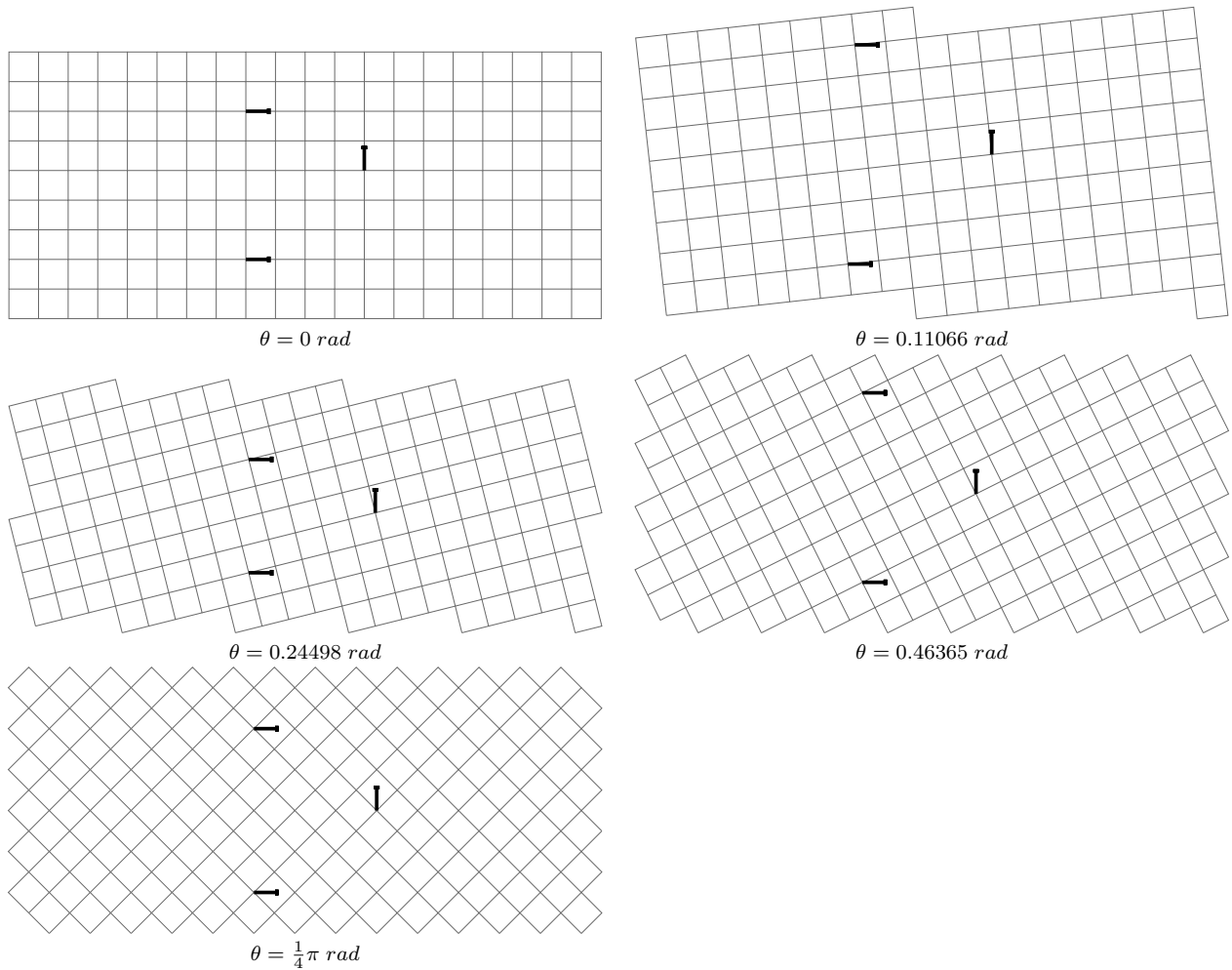


**Figure 6:** Uniform meshes (including supports) with five different mesh alignments or element orientations.

To present the results of the 15 analyses in a compact way, an outcome  $G_f^*$  is introduced. This *apparent* fracture energy is defined by

$$G_f^* = \int_0^{w_{ult}} \frac{F_x}{L_y t} du_{tot} \quad (1)$$

Eq. (1) indicates the area under the numerically obtained load - displacement curve for the range  $0 \leq u_{tot} \leq w_{ult}$ , divided by the theoretically expected crack area  $L_y t$ . Subsequently, the ratio  $G_f^*/G_f$  is calculated for all the 15 analyses and plotted against the element orientation angle  $\theta$ . This ratio can be seen as a measure for the deviation of the numerically obtained material fracture energy to the specified material fracture energy. The values are shown in the graph of Fig. 7.

It can be observed that the actual ratio of  $G_f^*/G_f$

for all analyses ranges from approximately 0.5 to 1.9. A scatter is already seen for  $\theta = 0$ . Where the curves belonging to the quadratic quadrilaterals converge subsequently with increasing  $\theta$ , the curve ‘quads, linear,  $2 \times 2$  Gauss’ deviates more and more from these two lines. Furthermore, it can be observed that the dashed lines in the graph are generally increasing with an increasing  $\theta$  - value. Only for the two quadrilateral element types with quadratic interpolation the curves show after approximately  $\theta = \pi/8$  a plateau until  $\theta = \pi/4$ .

Fig. 8 shows three crack width plots at  $u_{tot} \approx w_{ult}$  for the analyses with  $\theta = 0.24498$  rad and varying quadrilateral element types. Irrespective of the element type the plots reveal global cracks that clearly propagates along the inclined mesh lines, rather than vertically.

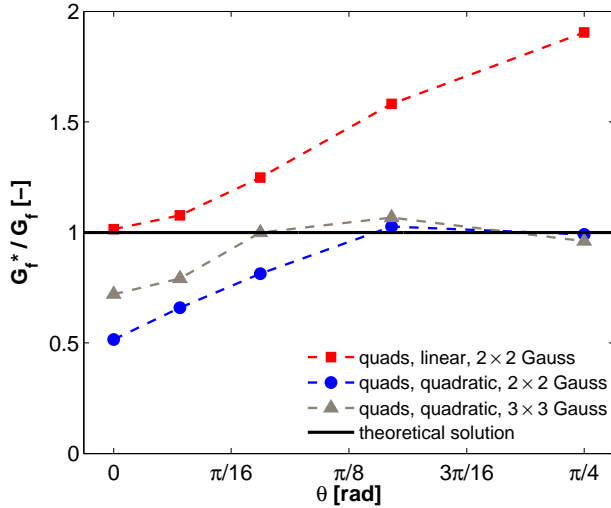


**Figure 7:** Deviation of the obtained apparent fracture energies  $G_f^*$  to the material fracture energy  $G_f$ .

On the other hand, the directions of the local cracks in the elements of the final localization zone are generally vertical. The widths of the localization zones in the plots are different, varying from half the element width (‘quads, quadratic,  $2 \times 2$  Gauss’) to the entire element width (‘quads, linear,  $2 \times 2$  Gauss’). Striking is the observed periodicity in the deformed meshes in both the crack patterns and opposite boundary displacements. This reveals that the periodic boundary conditions are properly applied.

The above mentioned observations from the Figs. 7 and 8 indicate that the band model according to Govindjee et al. suffers from a significant directional mesh bias, depending on interpolation function and numerical integration scheme. Ideally, the curves of the three element types in Fig. 7 should be horizontal lines at  $G_f^*/G_f = 1.0$ . However, they show a significant spread around this target line. Considering Fig. 6 and the trend of the curves in Fig. 7, the results of the analyses reveal that generally with an increasing misalignment of the cracks with respect to the element edges, the value  $G_f^*$  also increases. The difference in computed ratios at already  $\theta = 0$  can be explained by the phenomenon of strain localization within only a part of the element width rather than the entire element width. This happens only for the

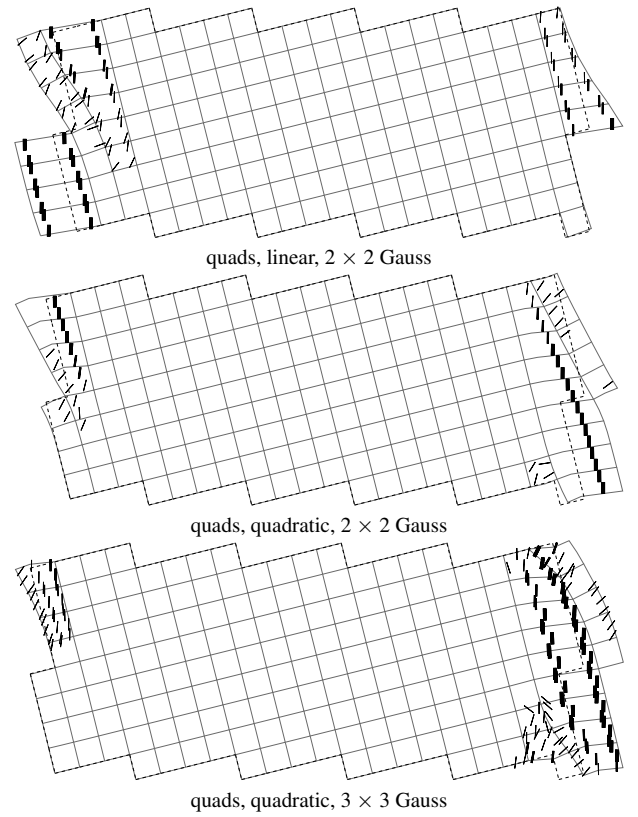


**Figure 8:** Crack width plots (deformed meshes) at  $\approx u_{tot} = 0.528\text{mm}$  belonging to the analyses in Fig. 7 with  $\theta = 0.24498 \text{ rad}$  and varying quadrilateral element types. The thickest lines correspond to  $w \geq w_{ult}$ .

quadratic quadrilateral elements, since they allow a linear strain field within the element. Depending on the adopted integration scheme the strain localization bandwidth is limited to one column of integration points ( $2 \times 2$  Gauss scheme) or two columns of integration points ( $3 \times 3$  Gauss scheme). As mentioned above, the phenomenon of strain localization within only a part of the element is also observed in the crack width plots of Fig. 8. With respect to the adopted numerical integration scheme it can be seen that the differences in mesh bias for quadratic quadrilaterals remain relatively small. The observed plateaus between  $\pi/8$  and  $\pi/4$ , after monotonic increasing parts of the curves, indicate that quadrilateral elements with a quadratic interpolation function are able to break through the tendency of the guided crack developments along continuous mesh lines. Finally, it should be noted that the value 1.9 at  $\theta = \pi/4$  of the curve ‘quads, linear,  $2 \times 2$  Gauss’

resembles with the numerically obtained localization bandwidth of the analysis ‘rNR - hordijk - no imp.’ in Fig. 4.

#### 4 CONCLUSIONS

In the present study a dedicated numerical test with periodic boundary conditions is proposed that enables a systematic assessment of directional mesh bias of constitutive models, like the crack band approach, nonlocal and gradient-enhanced models. The test can be performed for two- or three-dimensional FE discretizations under different loading conditions. Since the test includes the concept of periodicity, strain localization can be studied in meshes with different alignments, without loss of mesh uniformity and without disturbances from the model boundaries. Assessment of the constitutive models on directional mesh bias with this test may lead to a better understanding of the influence of the involved parameters, and possibly to improvement of model’s ability to deal with it.

From an exploratory study with the proposed test it appears that the results of a standard incremental-iterative solution procedure and the SLA-method are in reasonably agreement. Furthermore, it is found that the use of Moelands & Reinhardt softening stimulates the occurrence of an immediate strain localization after the peak load has been reached.

The actual purpose of the test with periodic boundary conditions is demonstrated by means of a mesh alignment study. In this small study the crack band model is evaluated in the context of a two-dimensional plane stress situation with uni-axial tensile loading. From the results of the numerical tests a significant directional mesh bias is recognized. The well-known phenomenon of strain localization within only a part of the element width rather than the entire element width, in case of quadratic quadrilaterals, is also clearly identified with this test.

#### REFERENCES

[1] Jirasek, M., 2002. Objective modeling of strain localization. *Revue française de gé-*

*nie civil* **6**:1119-1132.

- [2] Bazant, Z.P., Oh, B.H., 1983. Crack band theory for fracture of concrete. *Material and Structures* **16**:155-177.
- [3] Zijl, W., Hendriks, M.A.N., 't Hart, C.M.P., 2002. Numerical homogenization of the rigidity tensor in hookes law using the node-based finite element method. *Mathematical Geology* **34**:291-322.
- [4] Slobbe, A.T., Hendriks, M.A.N., Rots, J.G. Systematic assessment of directional mesh bias with periodic boundary conditions: applied to the crack band model. *paper submitted*.
- [5] Slobbe, A.T., Hendriks, M.A.N., Rots, J.G., 2012. Sequentially linear analysis of shear critical reinforced concrete beams without shear reinforcement. *Finite Elements in Analysis and Design* **50**:108-124.
- [6] Govindjee, S., Kay, G.J., Simo, J.C., 1995. Anisotropic modelling and numerical simulation of brittle damage in concrete. *International Journal for numerical Methods in Engineering* **38**:3611-3633.
- [7] Oliver, J., 1989. A consistent characteristic length for smeared cracking models. *International Journal for numerical Methods in Engineering* **28**:461-474.
- [8] Hordijk, D.A., 1991. Local approach to fatigue of concrete. *Phd, Delft University of Technology*.
- [9] Reinhardt, H.W., 1984. Fracture mechanics of an elastic softening material like concrete. *Heron* **29**:1-42.
- [10] Rots, J.G., Belletti, B., Invernizzi, S., 2008. Robust modeling of RC structures with an ‘event-by-event’ strategy. *Engineering Fracture Mechanics* **75**:590-614.
- [11] Jirasek, M., Zimmermann, T., 1998. Analysis of rotating crack model. *Journal of Engineering Mechanics* **124**:842-851.

- [12] Rots, J.G., Invernizzi, S., Belletti, B., Hendriks, M.A.N., 2009. Circumventing bifurcations in structural softening. In Max Hendriks, Sarah Billington (eds), *Computational Modeling on Concrete, Masonry and Fibre reinforced Composites*, Delft University of Technology; pp. 49-52.